

Cite this: *Soft Matter*, 2011, **7**, 7832

www.rsc.org/softmatter

PAPER

Capillary levelling as a probe of thin film polymer rheology

Joshua D. McGraw, Nicholas M. Jago and Kari Dalnoki-Veress*

Received 15th February 2011, Accepted 8th April 2011

DOI: 10.1039/c1sm05261f

While measuring the rheology of bulk polymer systems is routine, when the size of a system becomes comparable to molecular dimensions, properties of flow are hard to measure and poorly understood. We present the results of experiments that are easily performed and can probe the rheological properties of polymer films that are mere tens of nanometres in thickness. Glassy bilayer polymer films are prepared with height profiles well approximated by a step function. Upon annealing such stepped bilayer films above the glass transition, the height profiles broaden due to gradients in the Laplace pressure. By varying the molecular weights of the stepped films, we control the rate at which the broadening takes place. A scaling relation derived in the lubrication approximation is used to show that the rate of broadening is consistent with that expected from polymer rheology in the bulk, thus validating the technique as a uniquely versatile rheological probe for thin polymer films.

Introduction

Molecular mobility in confined environments is markedly different from that in the bulk. The study of confined flows has received considerable attention as the application of thin liquid films becomes relevant to industrial processes. Specifically, when a polymer melt is confined to length scales smaller than the natural size of these long chain molecules in the bulk, material properties change. These changes pose great challenges for our fundamental understanding of these systems. For this reason developing robust experimental methods for the study of flow in confined environments is an important endeavour; here we wish to make a contribution to this end.

Two notable experimental methods by which one can study the viscous and viscoelastic response of polymers confined to nanoscale dimensions are by the observation of dewetting liquid films from a substrate^{1–9} and the evolution of small scale surface structure.^{10–17} In the case of the former, much has been accomplished in understanding the fundamental processes that govern the dynamics of hole nucleation and growth. Dewetting in thin films proceeds because there can be a reduction of the free energy by exposing the underlying substrate. The energy gained by exposing the substrate is dissipated by viscous friction in a rim that forms around the dewetting hole. Fruitful collaboration between theory^{1,4,18–20} and this experimental technique has led to alternative measurements of the polymer reptation time,⁵ an improved understanding of the mechanisms controlling slip effects at the substrate polymer interface,^{7,8} and insight into the effect of film preparation on the rheology of thin polymer films.⁹

In addition to dewetting, hole growth in free standing polymer films has also been shown to be a valuable method of probing viscoelasticity of thin polymer films.^{21–23}

In the case of liquids which do not dewet a substrate and have some surface topography, there is an energy reduction due to a free surface evolution. Excess surface area is reduced by the Laplace pressure and the relaxation of the surface is moderated by viscous losses.^{10,24–26} The Laplace pressure arises from local curvature at the free surface, ρ , and is equal to $p = \gamma/\rho$, where γ is the surface tension.²⁴ In cases where lateral length scales are much greater than vertical ones, which is the case we will consider here, the inverse of the radius of curvature is simply given by the second derivative of the height with respect to position, $1/\rho \approx \partial_x^2 h$. Various experimental systems have been developed to study the relaxation of local curvature to investigate viscous, elastic and glass transition effects.^{11–17}

The measurement we describe here is among the list of rheological experiments that take advantage of surface tension to measure viscous properties of thin polymer films. In what is to follow, we will describe the technique which relies on preparing *stepped bilayer films* for the study of thin film rheology. The resulting samples are prepared in the glassy state and transition from a ‘thin’ to ‘thick’ region with an initial height profile that is well described by a Heaviside step function. As shown schematically in Fig. 1(a), the stepped films are composed of a film with thickness h_1 at the substrate, partially capped with a second film of thickness h_2 . A jump in temperature to above the glass transition, T_g , allows the system to relax. The relaxation proceeds such that the excess surface area in the transition from a thin film with thickness h_1 to a thick film with thickness $h_1 + h_2$ gradually disappears under the influence of surface tension. As shown in Fig. 1(b), we characterize the evolution of the surface profile with the width, w , which is a dominant length scale

Department of Physics & Astronomy and the Brockhouse Institute for Materials Research, McMaster University, Hamilton, ON, Canada.
E-mail: dalnoki@mcmaster.ca

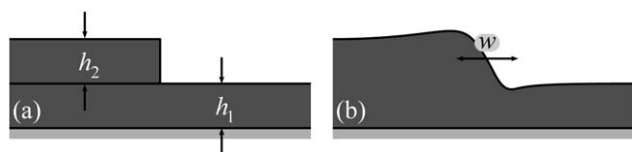


Fig. 1 Schematic diagrams of the sample geometry. (a) The as-prepared glassy stepped films composed of two layers: one in contact with the substrate of height h_1 and a second partially covering the first with height h_2 . (b) When the temperature is above T_g , the films are in the melt state and the width, w , spanning the regions between 'thin' (h_1) and 'thick' ($h_1 + h_2$) broadens.

describing the flow. Since the force of surface tension driving flow is balanced by viscous stresses, varying the molecular weight of the polymer used in the bilayers modifies the viscous damping. While our approach is complementary to the techniques described above, it is distinct in its ease and versatility. Here we consider the simplest case of two layers composed of a single polymer species with the same molecular weight. However, it is a simple matter to extend this technique to heterogeneous stepped films: two films of differing molecular weight, differing chain architecture (*e.g.* linear and branched), or chemically distinct polymer species, to name a few.

Experiment

All samples discussed in this work were prepared such that both films making up the stepped bilayer were prepared from polystyrene (PS) of the same molecular weight. The PS used had weight averaged molecular weights, $M = 24.7, 55.5$ and 118 kg mol^{-1} , with polydispersity indices of 1.03, 1.07 and 1.05 (Polymer Source Inc.). The polymer was dissolved in toluene with concentrations ranging from 1.0 to 3.9 wt% depending on the molecular weight of the polymer and the desired film thickness. In the first stage of the stepped bilayer preparation (see Fig. 2) a film with thickness approximately $h_1 = 100 \text{ nm}$ was spincast onto a $10 \times 10 \text{ mm}^2$ Si wafer (University Wafer). A second film also with an approximate thickness of $h_2 = 100 \text{ nm}$ was spincast onto a freshly cleaved $25 \times 25 \text{ mm}^2$ mica substrate (Ted Pella Inc.). Both films were annealed at $120 \text{ }^\circ\text{C}$ in vacuum for approximately 12 h to remove residual stress and solvent. After

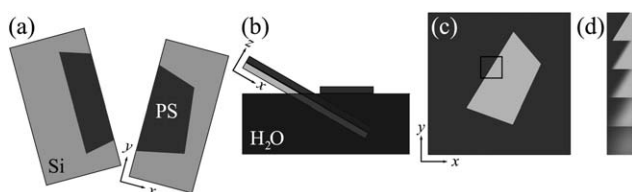


Fig. 2 Schematic diagrams illustrating steps of the sample preparation. (a) A PS film is floated from mica onto a bare Si wafer, which is then split in half. (b) One piece of PS, from (a) is floated off of the Si and onto a water bath. This portion of the PS film is then picked up using a thin film of PS that has been spincast onto a Si wafer. (c) The resulting stepped bilayer film, composed entirely of PS on a Si substrate, shows different light intensity under optical microscopy due to the differences in optical path length of the monolayer and bilayer region. (d) Schematic sequence showing that the transition in film thickness of the boxed film portion shown in (c) broadens upon annealing above T_g .

the initial annealing step, portions approximately $8 \times 8 \text{ mm}^2$ of the film which was spincast onto mica were floated onto a clean water bath (Milli Q). These pieces were then picked up using another $10 \times 10 \text{ mm}^2$ Si wafer. A section near the edge of the Si was previously scratched using a diamond scribe along the crystal axis prior to floating. Immediately after picking up these portions of the film, the diamond scribe was used to press firmly on the scratch near the edge of the Si wafer. The pressure induces fracture of the Si wafer along a line of crystal symmetry. With the film floated across this line, the procedure results in a polymer film with a straight edge (see Fig. 2(a)). Having prepared a thin film with a straight fracture, these portions of the film are again floated onto the clean water bath and subsequently picked up using the Si wafers which have had thin PS films previously spincast and annealed (Fig. 2(b)). With this procedure, it is possible to find portions of the bilayer polymer film with height profiles that are well approximated by a Heaviside step function, $h(x) = h_1 + h_2$ if $x < 0$, and $h(x) = h_1$ otherwise, where $h(x)$ is the film height at position x ; this stage of the preparation is shown in Fig. 1(a) and 2(c). The portions with straight edges are easily found using an optical microscope.

Prior to measurements on the surface profile evolution (see schematic in Fig. 2(d)) the step heights were measured using an atomic force microscope (AFM, Veeco Caliber) in tapping mode as follows. A scalpel blade was used to make a scratch down to the hard Si substrate, away from the region where the surface profile is to be observed. An AFM image in the region where the substrate is exposed could then be used to determine the thickness h_1 ; h_2 was subsequently determined by AFM in the region where the sample was to be observed using optical microscopy.

The prepared bilayers were placed on a heating stage (Linkam) in air and the temperature was rapidly increased ($90 \text{ }^\circ\text{C min}^{-1}$) from room temperature to $180 \text{ }^\circ\text{C}$, which is well above the glass transition of PS, $T_g \sim 100 \text{ }^\circ\text{C}$ (we have verified that performing the experiment in an inert argon atmosphere using a 52 kg mol^{-1} sample produces identical results to similar samples annealed in air). Shortly after reaching the final annealing temperature, optical microscopy images were collected at various intervals up to annealing times of approximately $6.6 \times 10^4 \text{ s}$. An optical filter centred at 630 nm (Newport 20BPF10-630, FWHM $\sim 10 \text{ nm}$) was placed between the light source and the sample so that, to a good approximation, all light reaching the CCD was monochromatic.

Under monochromatic illumination the light intensity observed in the optical images is a direct consequence of thin film interference.²⁷ In order to calibrate the thickness obtained from the light intensity values measured using the CCD camera, we prepared a series of thin PS films on $10 \times 10 \text{ mm}^2$ Si wafers. The thickness of all films was measured using ellipsometry. These eighteen films prepared ranged from 13 nm to 200 nm in thickness, bridging the range of thicknesses relevant to this study. Prior to each measurement of the surface profile evolution, a set of images was taken at the same exposure time and light intensity using the calibration samples so that, using an appropriate phase contrast model,²⁷ the intensity could be related to the thickness of the samples (see appendix).

For speed, versatility, and ease, measurements were performed with optical microscopy. However, the optical measurements

were verified using AFM. A sample with a molecular weight of 118 kg mol^{-1} was used to prepare a step edge as described above. The initial height profile was measured in tapping mode, and the sample was then heated to $180 \text{ }^\circ\text{C}$ for ten minutes. Following a quench to room temperature, the topographic data in the area of interest was again measured in tapping mode. This procedure was repeated several times for various annealing times up to an annealing time of approximately $4 \times 10^4 \text{ s}$.

Results and discussion

Atomic force microscopy

In Fig. 3, we show AFM topographic data for lines perpendicular to the step edge of a bilayer film. At $t = 0.04 \text{ s}$, our claim that the as-prepared bilayer film height profile is well represented by a Heaviside step function is verified. As time progresses, the transition region from thin to thick broadens. In addition, a prominent dip forms which falls below the thin portion of the stepped film. The dip is the result of material flow towards the low pressure region, thus depleting material from the thin portions. To characterize the width of the transition region, we obtain the tangent to the topographic data at position x_0 , where the height is half way between the thick and thin region $h_0 = h_1 + \frac{1}{2}h_2$. The width of the transition region can then be defined through the slope of the tangent line, $\partial_x h|_{x_0}$, as

$$w \equiv h_2(\partial_x h|_{x_0})^{-1}. \quad (1)$$

Defined in this way, w is the distance over which the extrapolated tangent of the $h(x)$ data at (x_0, h_0) traverses a height h_2 . The inset of Fig. 3 shows the temporal evolution of widths as measured by AFM. We note that the first data point corresponding to the as-prepared bilayer film is shown at $t = 0.04 \text{ s}$. This value for the time requires some justification.

As will be discussed below, the data is expected to follow a power law, $w(t) = bt^n$ with t the annealing time, and

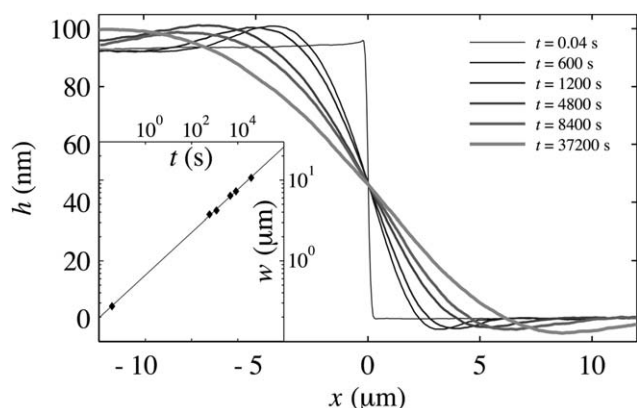


Fig. 3 AFM height profiles, horizontally shifted such that $h(x) = h_0$ when $x = 0$, of a 118 kg mol^{-1} PS stepped bilayer film annealed for various times up to $\sim 4 \times 10^4 \text{ s}$. The substrate is approximately 90 nm below the line extending horizontally from $x = 0$ through $x = 10 \text{ } \mu\text{m}$ in the AFM trace at $t = 0.04 \text{ s}$. The inset shows the width (see eqn (1)) of the transition from thin to thick film regions as a function of time. The line is a power law fit as described in the text.

b a constant. However, the annealing time of the as-prepared film should not be taken as $t = 0$, because there is ambiguity in the initial state for two reasons: (1) the as-prepared stepped film will evolve even at room temperature due to the high initial Laplace pressure; and (2) while the as-prepared film may be well *approximated* as a Heaviside step function, it will deviate from that on the smallest length scales. Thus, we fit the power law with an offset, which is equivalent to suggesting that the film, which relaxed at room temperature, had evolved as if it was heated at $180 \text{ }^\circ\text{C}$ for 0.04 s . Clearly the functional form with $b = 0.7 \pm 0.2$ and $n = 0.26 \pm 0.02$ is an excellent fit to the data.

Optical microscopy

In Fig. 4 we show typical optical images of the same spot on a 24.7 kg mol^{-1} stepped film, both as-prepared (a), and after annealing for approximately $6.6 \times 10^4 \text{ s}$ (b). These images can be compared to the schematic evolution shown in Fig. 2(d) and the evolution of the AFM line profiles in Fig. 3. The contrast in the images is due to spatial variation of the optical path length resulting from differences in the film thickness. The solid white lines in Fig. 4(a) and (b) show the observed average intensity across the transition region. Consistent with the schematic and the AFM data, these images show that the transition between the thin and thick regions of the film broadens with time. In comparing AFM to optical microscopy data, it is worthwhile noting that while AFM has the advantage of being able to probe narrow transition widths, optical

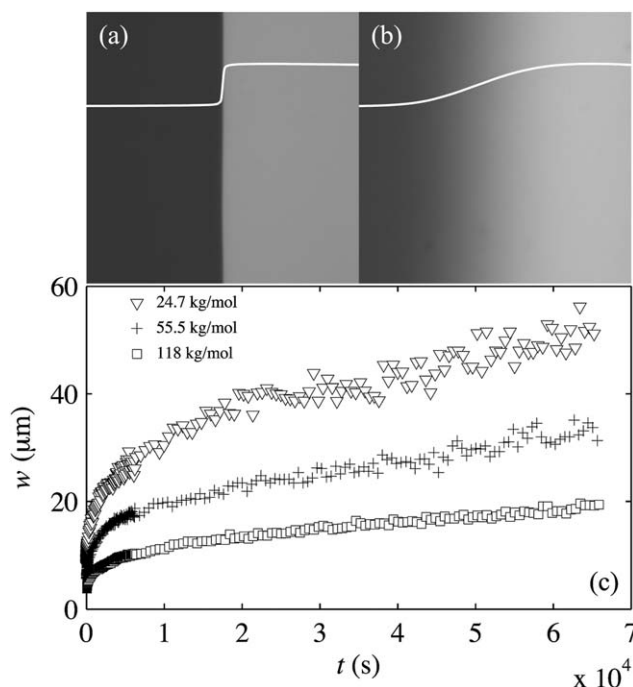


Fig. 4 (a) An optical image of an as-prepared 24.7 kg mol^{-1} PS stepped film; and (b), the same sample after annealing for approximately $6.6 \times 10^4 \text{ s}$. Optical microscopy images were obtained under monochromatic illumination. The solid white lines show the averaged intensity profile across the transition region. The width and height of both images is $65 \text{ } \mu\text{m}$. (c) The width, $w(t)$, for the transition region of the stepped films prepared from three different molecular weights. w was determined from the optical images and determined using eqn (6).

microscopy can access small gradients in the height. Remarkably this translates to being able to probe lateral flows over tens of micrometres in films with thickness ~ 100 nm. The geometry of this stepped film is such that the thin region is near the first minimum in the periodic thickness *versus* reflected intensity curve and the thick film is close to but less than the nearest maximum. Thus, the intensity varies monotonically with the film thickness, simplifying the interpretation of the images. Using the thin film interference equations to describe the reflected intensity as observed on the CCD detector,²⁷ it is straightforward to obtain w as described in the appendix.

Fig. 4(c) shows the results of several experiments in which stepped films were annealed for approximately 6.6×10^4 s at 180°C . From the intensity profiles of the monochromatically illuminated optical images the width was obtained as a function of time for three molecular weights (see eqn (6) in the appendix). For all samples studied, $w(t)$ increases quickly for early times, since that is when gradients in the Laplace pressure are the greatest. As the widths become larger, the rate of increase slows as the pressure gradients relax. It is notable that for a given annealing time, the molecular weight of the sample determines the width; larger molecular weights result in smaller widths due to the greater viscous dissipation.

To understand the data presented in Fig. 4(c) quantitatively, we resort to analysis based on the lubrication approximation of the Stokes fluid equations. Extensive reviews on flow in thin fluid films have been written^{25,26} and the evolution equations are developed there in full detail and for systems of much greater generality than we will consider here. Stillwagon and Larson¹⁰ have carried out a detailed derivation of flow in a system that is similar to that described here. Here we quote the final result, while their derivation is outlined in the appendix. Within the lubrication approximation, the width characterizing the transition region between the thin and thick regions of the film grows as a power law in time:

$$w^4 \sim \frac{\gamma h_0^3 t}{\eta}, \quad (2)$$

where η is the viscosity of the fluid under study.

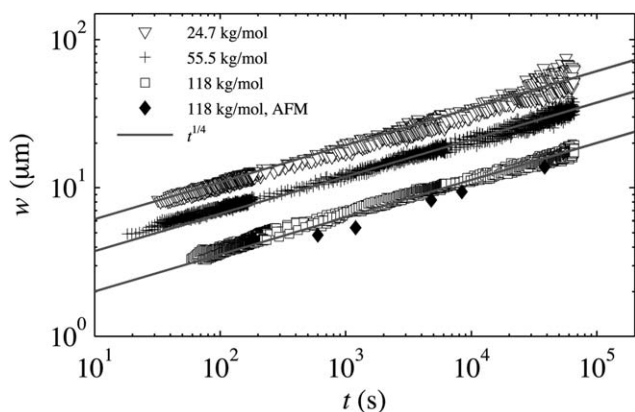


Fig. 5 Logarithmic plots showing w as a function of t for several stepped films. For each molecular weight, the data represent four individual annealed bilayers under similar conditions. Except for the sample that was observed by AFM (\blacklozenge), all samples were observed under an optical microscope.

Comparison to model expectations

In Fig. 5 we show the results of $w(t)$ for all stepped films on a double logarithmic plot in accordance with the prediction of eqn (2). As discussed above, there is some ambiguity in the choice of $t = 0$ because of sample preparation and relaxation of the step prior to commencing the experiment. Furthermore, experimental practicalities dictate that it takes some time to heat from below T_g to 180°C , to focus the sample, and begin data collection. For this reason all data are fit to the functional form for $w(t)$ with an offset in time to determine the time corresponding to the first width measurement point (*i.e.* shift t , such that when the data is extrapolated to $t = 0$, $w = 0$). The time shifts for all data are reasonable and range from 18 s to 120 s. Clearly this lag time only affects the initial annealing times and is insignificant for annealing times ranging up to tens of hours.

In addition to the optical data, we also show the widths as measured directly from the AFM profiles of Fig. 3. While all optical data was carried out for stepped films with nearly equal values of $h_0 = 148 \pm 3$ nm, the AFM images were obtained on films that were slightly thinner with $h_0 = 136 \pm 2$ nm. Thus the AFM data was scaled by the factor $(148/136)^3$ in accordance with eqn (2). The agreement between the AFM and optical data for the 118 kg mol^{-1} PS provides a further verification of the measurement and eqn (2).

Eqn (2) predicts that the measured width of annealing bilayers should increase with time as a power law, $w(t) = bt^{1/4}$. The solid gray lines in Fig. 5 are best fits to the data using b as the only fitting parameter for each molecular weight. The data is well represented by the expected power law dependence. As pointed out by Mullins,²⁸ there are additional surface and volume diffusion processes that may contribute to the evolution of the steps, especially in the case of small molecule liquid systems. Below we present analyses which supports the idea that bulk flow is a dominant mechanism for the results presented in Fig. 3–7.

The result from the lubrication approximation also predicts that the prefactor, b , should decrease with the viscosity as $\eta^{-1/4}$. The prefactor also contains dependence on γ and h_0 , but only the molecular weight, and hence the viscosity, varies between data

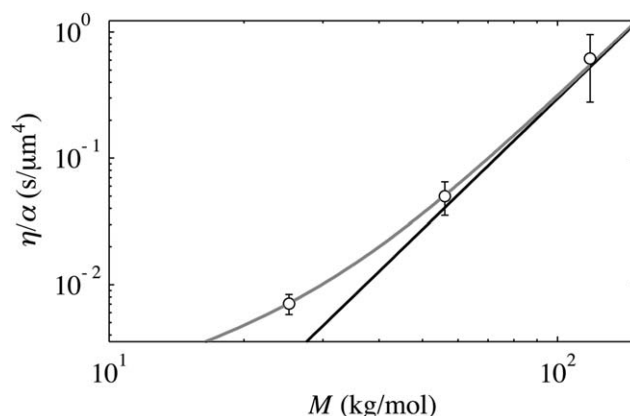


Fig. 6 Scaled viscosities, η/α , as a function of molecular weight obtained from the data in Fig. 5. The grey curve is the best fit of eqn (3), which describes $\eta(M)$ in the crossover region from Rouse dynamics ($\eta \sim M$) to the reptation dynamics in the entangled melt $\eta \sim M^{3.4}$. The black curve represents the long chain reptation regime.

sets in Fig. 5. Therefore, we can write $b = (\alpha/\eta)^{1/4}$, with α a constant. Since the viscosity of a polymer melt varies with molecular weight, M , in a well established manner,²⁹ it is possible to verify the scaling of the data with M as suggested by eqn (2).

In Fig. 6 we show the values of η/α as a function of the molecular weight, where η/α was obtained from the best fits to the data in Fig. 5. Since α is independent of the molecular weight, the ratio η/α should follow the well established dependence of the melt viscosity as a function of M (see the text by Rubinstein and Colby²⁹). For chains much shorter than the critical molecular weight, M_c , the viscosity of a polymer melt is dominated by the Rouse model. In this regime $\eta \sim M$. On the other hand, for $M \gg M_c$, entanglement effects are most important and in this regime it is found that $\eta \sim M^{3.4}$. It turns out that for polystyrene, the critical molecular weight is approximately $M_c \approx 31 \text{ kg mol}^{-1}$.³⁰ Therefore, the molecular weights used in this study are in neither asymptotic regime. In the crossover regime the viscosity is well described by²⁹

$$\eta \sim M \left[1 + \left(\frac{M}{M_c} \right)^{2.4} \right] \quad (3)$$

which smoothly joins the two asymptotic limits. Eqn (3) assumes that our experiments probe only the zero shear rate viscosity. This assumption is justified here by ensuring that our strain rate is well below that for which shear thinning becomes important.†

The gray solid line in Fig. 6 shows the best fit curve to the η/α data using eqn (3). In this fit there is only one free parameter in the expression $\eta/\alpha = \zeta M [1 + (M/M_c)^{2.4}]$. We find $\zeta = 1.8 \pm 0.5 \times 10^{-4} \text{ mol s kg}^{-1} \mu\text{m}^4$. Also shown (black line) is the extrapolated high molecular weight asymptotic limit with $\eta \sim M^{3.4}$. The agreement with the expected functional form is excellent, providing further evidence that the technique is a robust probe of viscosity in thin polymer films. As noted above, the prefactor, b , of eqn (2) contains dependence on the height, the surface tension of the films, and a numerical constant. Taking the height as h_0 , using the surface tension of polystyrene³³ and bulk viscosities³² corrected for temperature using the WLF equation,²⁹ we can extract an estimate of the numerical constant by considering the data in Fig. 6. Eqn (2) is thus empirically determined to be $w^4 = (9 \pm 2)\gamma h_0^2 t/\eta$ for these experiments.

Having demonstrated that the experimental results are well described by the expected dependence of the width of the transition on time and viscosity through the use of eqn (2) and (3), it is possible to produce a master curve of all the w versus t data in Fig. 5. In Fig. 7 we show all measured widths plotted as a function of at/η with the scaling factors as in Fig. 6. The data collapses onto a single master curve that spans five orders of magnitude in scaled time and more than one order of magnitude in the width. The existence of such a curve allows the levelling times of geometrically similar films annealed at 180 °C to be

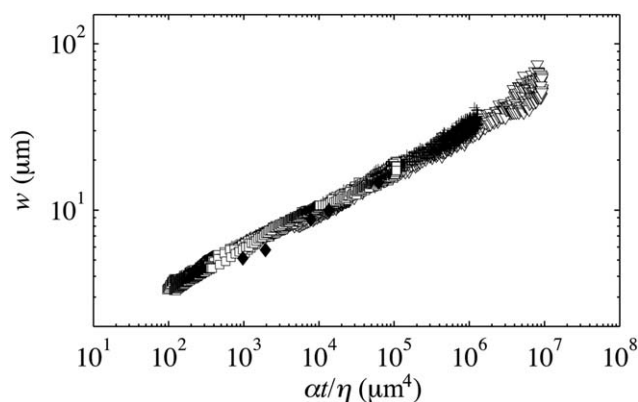


Fig. 7 Measured widths as defined in eqn (6) as a function of the scaled time at/η . The symbols are as in Fig. 5.

predicted for a range of molecular weights (viscosities) using eqn (3). Eqn (3) can be used only when the assumption that polymers are in their bulk configuration is valid. This assumption is valid for the films studied here which are much thicker than the radius of gyration of the molecules studied. Polymers in confinement can be investigated by preparing films that are much thinner than the radius of gyration. Preliminary measurements indicate that an observable departure from the bulk expectation (eqn (3)) can be measured using this technique. Measurements of this type will be the subject of a future work.

We end the discussion with a short comparison of our experiment with dewetting experiments of the type that were briefly discussed in the introduction. The rheological studies in which a thin liquid film dewets a substrate have made major contributions to the understanding of many fundamental aspects of polymer science. However, by the very nature of the dewetting problem, it depends on the presence of a surface that is unfavourable for the homogenous liquid that rests upon it. The approach presented here addresses some of the limitations of dewetting studies. While we have focussed on simple homogenous polymer films, by simply changing the two individual films used to prepare the stepped bilayers, it is straightforward to study a wide variety of two component systems. For example the molecular weight, chain architecture, or even the chemical species of the two films that make up the stepped geometry need not be the same. Additionally, the excellent resolution of the film thickness over large length scales possible with optical microscopy under monochromatic illumination provides further opportunities. In particular, measurements of $w(t)$ on films with a constant step height h_2 , and varying thin region h_1 , are sensitive to the polymer substrate boundary condition (*i.e.* lubrication approximation and slip effects). In contrast, varying the step height while keeping the underlying film constant is sensitive to the polymer air interface—a topic that has received tremendous recent attention.

Conclusion

Here we have presented an experimental methodology for the measurement of rheological properties of thin polymer films. Through relatively simple sample preparation procedures, stepped bilayer films are prepared in the glassy state by floating a film with thickness h_2 to partially cover a film of the same polymer with thickness h_1 supported on a substrate. The height profile varies along a line providing a simple

† The dimensionless shear strain rate to be considered is³¹ $\beta = \eta M \dot{\epsilon} / \rho R T$ where $\dot{\epsilon}$ is the shear strain rate, ρ is the mass density and R is the molar gas constant. The largest strain rate in our experiments can be estimated from the early time data of Fig. 4 as $\dot{\epsilon} = \Delta w / h_0 \Delta t \approx 0.1 \text{ s}^{-1}$ for 118 kg mol^{-1} . Using the known viscosity at the temperature at which the experiment is carried out³² an estimate of β can be made. Here β never exceeds 0.02. Since the viscosity is independent of $\dot{\epsilon}$ for $\beta < 1$,³¹ a zero shear rate viscosity is probed in the measurements presented.

flow experiment when the sample is brought into the melt regime. For these thin films gravitational effects can be neglected and the flow is only driven by the Laplace pressure caused by the curvature at the step. The geometry is analytically and experimentally convenient, as well as easy to prepare. Optical microscopy with the sample illuminated by monochromatic light proves to be a simple way to measure the width of the transition from the thin to thick regions of the film. In this first investigation, we have focussed on a well characterized and understood problem: the molecular weight dependence of bulk polymer viscosity. It was shown that the method can be used to measure the differences in the viscosity of a polymer melt as the molecular weight changes. While this study establishes the stepped film geometry as a robust system for the measure of rheological properties in thin films, we are hopeful that the technique will motivate future experiments on more exotic systems.

Appendix

Obtaining $w(t)$ from optical measurements

While in practice one could empirically obtain the calibration factor that translates from a gradient in intensity to a gradient in thickness, here we have used a more rigorous approach. Using thin film equations to describe the reflected intensity as observed on the CCD detector, we can get a measurement of w . Since the height profiles of the thin films are always slowly varying with position we assume that the reflected intensity, I , at position x is a function only of the local height, that is $I = I(h)$. For a uniform transparent film the reflectance is given by²⁷

$$R(h) = \frac{A - B + C \cos(2kh)}{A + B + C \cos(2kh)}, \quad (4)$$

with,

$$\begin{aligned} A &= (n_a^2 + n_p^2)(n_p^2 + n_s^2), \\ B &= 4n_a n_p^2 n_s, \\ C &= (n_a^2 - n_p^2)(n_p^2 - n_s^2), \\ k &= 2\pi n_p / \lambda, \end{aligned}$$

where the wavelength, $\lambda = 633$ nm, is determined by the choice of optical filter, n_a , n_p and n_s are the refractive indices of the air, PS and substrate (here we have taken $n_a = 1$, $n_p = 1.56$ and $n_s = 3.9$). For all of the experiments reported here, the only variable is the film thickness and all other parameters in eqn (4) can be taken as constant. Since even at minimum reflectance there is some background light that makes it to the detector, we model the intensity at the CCD as

$$I(h) = I_b + I_r R(h), \quad (5)$$

where I_b and I_r are fitting parameters. We note that prior to any analysis of the surface profiles (Fig. 4(a) and (b)), the standard PS films with known thicknesses were imaged, their average intensity plotted as a function of h , and the data fit to $I(h)$ to determine the fitting parameters I_b and I_r . This procedure ensured a quick and robust calibration of the relationship between intensity and film thickness. Once calibration images were obtained, all measurements on the stepped films were carried out with the same exposure time and light intensity.

From the definition of the width of the transition in the stepped films as given by eqn (1) and using eqn (4) and (5), we get

$$w \equiv h_2 (\partial_x h|_{x_0})^{-1} = h_2 \left(\frac{\partial_x I|_{x_0}}{I_r \partial_h R|_{h_0}} \right)^{-1}. \quad (6)$$

All derivatives are evaluated at the position where the height of the film is exactly half way along the step (x_0 , h_0). All the quantities on the right hand side of eqn (6) are easily accessible in the measurements performed, and the gradient of the intensity half way up the step, $\partial_x I|_{x_0}$, is the only time dependent quantity. This method of determining the widths can be used when $w \geq \lambda$. For the setup we have used, we can measure widths larger than approximately 1 μm . As seen in Fig. 4(c), none of the widths reported in this study violate this limitation.

Scaling prediction for $w(t)$ from the lubrication approximation

The following calculation is done in greater generality elsewhere,^{10,25,26} but for completeness we outline the main steps in the derivation of the scaling of the width of the transition region with time, $w(t)$. Here, we do not consider gravitational or long range (e.g. van der Waals) forces, evaporation/condensation, or surface tension gradients. Stillwagon and Larson¹⁰ have derived, and experimentally verified, the flow equations based on the lubrication approximation for substrate topographies that are not necessarily flat. Their detailed calculation can be further simplified because our substrates are flat. For the system discussed here, all of the above assumptions are valid and the Stokes equation for the flow in one dimension is

$$0 = \partial_x p + \eta \partial_z^2 u, \quad (7)$$

where p is the pressure, η is the viscosity, u is the velocity in the horizontal direction and z is the vertical coordinate. Assuming no slip at the boundary between the film and the substrate, that there is no stress supported at the air–polymer interface, and that the pressure does not vary in the vertical direction, a parabolic velocity profile in the z -direction results.^{10,24} Since the velocity profile is quadratic with respect to the vertical coordinate and assuming an incompressible fluid, the volume flow rate is cubic in the local film height, $h(x)$. With eqn (7) we then obtain the volume flow rate per unit film width $Q = -h^3 \partial_x p / 3\eta$. The pressure is the product of the surface tension and the curvature at the air–polymer interface. Since $\partial_x h \ll 1$ for all the samples observed under optical microscopy, the pressure is well approximated by $p = \gamma \partial_x^2 h$. Imposing conservation of mass gives an evolution equation for the height profile as a function of time. For the system we are considering, the lubrication approximation for the temporal evolution of this height profile is

$$\partial_t h = \frac{\gamma}{3\eta} \partial_x (h^3 \partial_x^3 h). \quad (8)$$

Nondimensionalizing eqn (8) gives a relevant time scale that is a function of the relevant length scales, the surface tension and the viscosity: $t \approx w^4 \eta / \gamma h_0^3$. Upon rearranging for the width

$$w^4 \approx \frac{\gamma h_0^3 t}{\eta}, \quad (9)$$

as shown in eqn (2). Here we have assumed that the relevant height scale in the problem is h_0 , while the x direction it is the width, w .

Acknowledgements

Financial support from NSERC of Canada is gratefully acknowledged. The authors thank Professors J. A. Forrest and A-C. Shi for valuable discussions.

References

- 1 F. Brochard Wyart and J. Daillant, *Can. J. Phys.*, 1990, **68**, 1084.
- 2 G. Reiter, *Phys. Rev. Lett.*, 1992, **68**, 75.
- 3 R. Seemann, S. Herminghaus and K. Jacobs, *Phys. Rev. Lett.*, 2001, **87**, 196101.
- 4 J. Becker, G. Grün, R. Seemann, H. Mantz, K. Jacobs, K. Mecke and R. Blossey, *Nat. Mater.*, 2002, **2**, 59–63.
- 5 S. Gabriele, S. Slavovs, G. Reiter and P. Damman, *Phys. Rev. Lett.*, 2006, **96**, 2006.
- 6 D. Bonn, J. Eggers, J. Indekeu, J. Meunier and E. Rolley, *Rev. Mod. Phys.*, 2009, **81**, 739.
- 7 O. Baumchen, R. Fetzer and K. Jacobs, *Phys. Rev. Lett.*, 2009, **103**, 247801.
- 8 G. Reiter, S. Akhrass, M. Hamieh, P. Damman, S. Gabriele, T. Vilmin and E. Raphaël, *Eur. Phys. J. Spec. Top.*, 2009, **166**, 165.
- 9 A. Raegen, M. Chowdhury, C. Calers, A. Schmatulla, U. Steiner and G. Reiter, *Phys. Rev. Lett.*, 2010, **105**, 227801.
- 10 L. Stillwagon and R. Larson, *J. Appl. Phys.*, 1988, **63**, 5251.
- 11 T. Kerle, Z. Lin, H.-C. Kim and T. Russell, *Macromolecules*, 2001, **34**, 3484.
- 12 E. Buck, K. Petersen, M. Hund, G. Krausch and D. Johannsmann, *Macromolecules*, 2004, **37**, 8647–8652.
- 13 T. Leveder, S. Landis and L. Davoust, *Appl. Phys. Lett.*, 2008, **92**, 013107.
- 14 Z. Fakhraai and J. Forrest, *Science*, 2008, **319**, 600.
- 15 D. Barbero and U. Steiner, *Phys. Rev. Lett.*, 2009, **102**, 248303.
- 16 M. Ilton, D. Qi and J. Forrest, *Macromolecules*, 2009, **42**, 6851–6854.
- 17 J. Teisseire, A. Revaux, M. Foresti and E. Barthel, *Appl. Phys. Lett.*, 2011, **98**, 013106.
- 18 P. de Gennes, *Rev. Mod. Phys.*, 1985, **57**, 287.
- 19 V. Shenoy and A. Sharma, *Phys. Rev. Lett.*, 2002, **88**, 236101.
- 20 T. Vilmin and E. Raphaël, *Europhys. Lett.*, 2005, **72**, 781.
- 21 G. Debrégeas, P. Martin and F. Brochard-Wyart, *Phys. Rev. Lett.*, 1995, **75**, 3886–3889.
- 22 K. Dalnoki-Veress, B. Nickel, C. Roth and J. Dutcher, *Phys. Rev. E*, 1999, **59**, 2153.
- 23 C. Roth and J. Dutcher, *J. Polym. Sci., Part B: Polym. Phys.*, 2006, **44**, 3011.
- 24 P. de Gennes, F. Brochard-Wyart and D. Quéré, *Capillarity and Wetting Phenomena: Drops, Bubbles, Pearls, Waves*, Springer, 2003, vol. 1.
- 25 A. Oron, S. Davis and S. Bankoff, *Rev. Mod. Phys.*, 1997, **69**, 931.
- 26 R. Craster and O. Matar, *Rev. Mod. Phys.*, 2009, **81**, 1131.
- 27 O. Heavens, *Rep. Prog. Phys.*, 1960, **23**, 1.
- 28 W. Mullins, *J. Appl. Phys.*, 1959, **30**, 77.
- 29 M. Rubinstein and R. Colby, *Polymer Physics*, Oxford University Press, 2003.
- 30 L. Fetters, D. Lohse, S. Milner and W. Graessley, *Macromolecules*, 1999, **32**, 6847.
- 31 W. Graessley, *Adv. Polym. Sci.*, 1974, **16**, 1.
- 32 T. Fox and P. Flory, *J. Am. Chem. Soc.*, 1948, **70**, 2384.
- 33 D. Schrader, *Polymer Handbook*, John Wiley & Sons, Inc., 1999, vol. 4, ch. V, p. 91.